Application of the v^2-f model to aerospace configurations

By Georgi Kalitzin

1. Motivation and objectives

Reynolds-Averaged Navier-Stokes (RANS) methods have become an important design tool in aerospace industry. Turbulence models, which are required for closure of the RANS equations, are a substantial component in these methods. Several flow regimes exist where the accuracy of flow predictions depends strongly on the turbulence model used.

Turbulence has a major influence on the growth rate of boundary layers for flow around airfoils. In subsonic flows at high-lift conditions, strong adverse pressure gradients decelerate the flow. The turbulence intensity in the flow directly affects separation of the flow. In transonic flows the boundary layer growth influences the location of shock waves. Generally, a more rapid growth moves shocks further upstream. Depending on location and strength, a shock may induce separation of the flow. Flow separation strongly affects the lift and drag of an airfoil as a consequence of a change in the circulation around the airfoil. These examples, test cases for which are considered in this report, demonstrate the need for accurate turbulence models.

The objective of the present report is to evaluate the v^2-f model (Durbin 1995) for aerospace applications. Different versions of this model are validated on flow around single- and multi-element airfoils. The flow predictions are compared with experimental data and results obtained with the Spalart-Allmaras (Spalart & Allmaras 1992) and Menter SST (Menter 1993) models. Both models are widely used in aerospace industry. While comparison with experimental data provides a measure for the physicality of the results predicted, the comparison with other turbulence models provides a competitive measure of accuracy.

2. Accomplishments

2.1 Numerical method

The present results have been computed with the NASA code CFL3D version 5 (Krist *et al.* 1997). This is a compressible, finite-volume RANS code for multi-block structured grids. Turbulence models are solved in this code segregated from the mean flow in an implicit manner using a three-factored Approximate Factorization scheme with an explicit treatment of the boundary condition. The v^2-f model has been implemented into CFL3D in a similar fashion (Kalitzin 1997, 1998). The model's transport equations are solved, however, in an implicit pairwise coupled manner with an implicit treatment of the wall boundary conditions. A three- and

two-factored Approximate Factorization scheme is used for the solution of the linear algebraic system of equations which results from the implicit treatment of the equations.

2.2 Durbin's v^2-f turbulence model

Two versions of the v^2-f model have been developed since its first introduction by Durbin in 1995. These originated from the desire to eliminate the use of wall distance and to improve the numerical behavior related to the stiffness of the wall boundary conditions for ϵ and f. A summary of the different versions is given to demonstrate the differences in the models.

Model 1: The equations of the original v^2-f model (Durbin 1995) for compressible flow are:

$$\partial_t k = \frac{1}{\rho}\nabla\cdot[(\mu+\mu_t)\nabla k] - U\cdot\nabla k + P_k - \epsilon$$

$$\partial_t \epsilon = \frac{1}{\rho}\nabla\cdot\left[(\mu+\frac{\mu_t}{\sigma_\epsilon})\nabla\epsilon\right] - U\cdot\nabla\epsilon + \frac{C^*_{\epsilon 1}P_k - C_{\epsilon 2}\epsilon}{T}$$

$$\partial_t \overline{v^2} = \frac{1}{\rho}\nabla\cdot\left[(\mu+\mu_t)\nabla\overline{v^2}\right] - U\cdot\nabla\overline{v^2} + kf - \frac{\epsilon}{k}\overline{v^2} \tag{1}$$

$$f = L^2\nabla^2 f + \frac{C_1}{T}\left[\frac{2}{3} - \frac{\overline{v^2}}{k}\right] + C_2\frac{P_k}{k} \tag{2}$$

where ρ is the density, μ the dynamic viscosity, and U the mean velocity vector. P_k represents the production of turbulent kinetic energy due to the mean flow velocity gradients.

$$P_k = 2\nu_t S^2$$

The time and length scales are computed as

$$T = \min\left[\max\left[\frac{k}{\epsilon}, 6\sqrt{\frac{\nu}{\epsilon}}\right], \frac{0.6k}{\sqrt{6}C_\mu\overline{v^2}S}\right]$$

$$L = C_L\max\left[\min\left[\frac{k^{3/2}}{\epsilon}, \frac{k^{3/2}}{\sqrt{6}C_\mu\overline{v^2}S}\right], C_\eta\frac{\nu^{3/4}}{\epsilon^{1/4}}\right]$$

The magnitude of the strain tensor is defined by $S=\sqrt{S_{ij}S_{ij}}$ with $S_{ij}=0.5(\partial u_j/\partial x_i + \partial u_i/\partial x_j)$. The eddy-viscosity is given by

$$\mu_t = C_\mu\rho\overline{v^2}T,$$

and the model's coefficients are:

$$C_{\epsilon 2}=1.9,\ \sigma_\epsilon=1.3,\ C_1=0.4,\ C_2=0.3,$$

$$C^*_{\epsilon 1}=1.3+0.25/[1+(C_L d/2L)^2]^4,\ C_\mu=0.19,\ C_L=0.3,\ C_\eta=70 \tag{3}$$

The wall boundary conditions enforce the correct near wall behavior of k and $\overline{v^2}$:

$$k_w = 0,\ \overline{v_w^2} = 0,\ \epsilon_w = \frac{2\nu k_1}{y_1^2},\ f_w = -\frac{20\nu^2\overline{v_1^2}}{\epsilon_w y_1^4} \tag{4}$$

The indices w and 1 denote the wall and first point above the wall, respectively.

Model 2: To eliminate the wall distance d, which is present in Eq. (3) for $C_{\epsilon 1}^*$, a new expression for the coefficient $C_{\epsilon 1}$ has been defined which uses the ratio $k/\overline{v^2}$ (Parneix & Durbin 1997). The new equation for $C_{\epsilon 1}$ and the new calibrated set of constants are:

$$C_{\epsilon 1} = 1.4(1 + 0.045\sqrt{k/\overline{v^2}}),\ C_\mu = 0.22,\ C_L = 0.25,\ C_\eta = 85 \tag{5}$$

Model 3: A second modification has been introduced to obtain a more numerically friendly version of the model. During the application of the v^2-f model to several wall bounded flows, it has been found that the numerical difficulties encountered are primarily connected with the strong coupling of the turbulence variables in the ϵ and f wall boundary condition, given in Eq. (4). The factor resulting from the power of y_1 can be rather large especially for high Reynolds number flows which require a finer mesh near the wall. The addition of an additional source term to the f-equation and the subtraction of a similar term from the $\overline{v^2}$-equation preserves the $\sim y^4$ behavior of $\overline{v^2}$ near the wall and leads to a simple wall boundary condition for a new variable $\tilde{f}$ (Lien & Durbin 1996). This facilitates an equation-by-equation solution approach which prohibits an implicit coupling of the wall boundary conditions.

In summary, the modifications to Model 1 are:

$$\partial_t\overline{v^2} + U\cdot\nabla\overline{v^2} = \frac{1}{\rho}\nabla\cdot\left[(\mu + \frac{\mu_t}{\sigma_k})\nabla\overline{v^2}\right] + k\tilde{f} - 6\frac{\epsilon}{k}\overline{v^2}$$

$$\tilde{f} - L^2\nabla^2\tilde{f} = \frac{C_1}{T}\left[\frac{2}{3} - \frac{\overline{v^2}}{k}\right] + C_2\frac{P_k}{k} + 5\frac{\overline{v^2}}{kT}$$

and

$$C_{\epsilon 1} = 1.4(1 + 0.045\sqrt{k/\overline{v^2}}),\ C_L = 0.23$$

The wall boundary condition for $\tilde{f}$ is: $\tilde{f}_w = 0$.

Note that the transport equations for $\overline{v^2}$ and $\tilde{f}$ can be derived from Model 1 by substituting f with $f^* - 5\epsilon\overline{v^2}/k^2$ and neglecting the term $-5L^2\nabla^2(\epsilon\overline{v^2}/k^2)$ which appears in the transformed f^*-equation. The ratio k/ϵ appearing in the new $\tilde{f}$-equation is substituted with the time scale T.

2.3 Subsonic and transonic flow around airfoils

Flow around three airfoils has been computed for subsonic and transonic flow conditions. The test cases considered are described in the next three sections. Section 2.3.4 discusses the results computed.

2.3.1 Subsonic two-element NLR7301-airfoil

Flow around the two-element NLR7301-airfoil (Van den Berg 1979) has been computed for $M = 0.185$, $Re = 2.51 \times 10^6$, and two flow incidences of $\alpha = 6.0^o$ and $\alpha = 13.1^o$. For the higher incident the flow is close to maximum lift condition. The gap between airfoil and flap is in both cases 2.6% and the flap deflection is $\delta_F = 20^o$. With the exception of a small laminar separation bubble upstream of transition, the flow is fully attached in both cases. In the $\alpha = 6.0^o$ case, transition occurred in the experiments at $0.027 - 0.040$ cord length on the upper surface and at $0.650 - 0.680$ on the lower surface of the wing as well as at $1.095 - 1.107$ (for a flap based coordinate system at $0.194 - 0.206$) on the upper surface of the flap. In the $\alpha = 13.1^o$ case, transition occurred correspondingly at $0.024 - 0.035$, at $0.710 - 0.740$, and at $1.069 - 1.084$ $(0.168 - 0.183)$. The patched, multiblock computational mesh consists of 36208 cells. It has been used as the mandatory mesh in ECARP (Haase *et al.* 1997).

2.3.2 Subsonic A-airfoil

Flow around the A-airfoil (Glayzes 1988, 1989) has been computed for the flow condition: $M = 0.15$, $Re = 2.0 \times 10^6$, and $\alpha = 13.3^o$. This flow condition is similar to the high-lift condition for the NLR 7301-airfoil. However, in this case experiments show a laminar separation bubble upstream of transition and a turbulent separated flow region near the trailing edge. In the experiments transition has been tripped at 12% on the upper surface and at 30% on the lower surface. The computational mesh used consists of 256x64 cells. It was again used as the mandatory mesh in ECARP (Haase *et al.* 1997).

2.3.3 Transonic RAE2822-airfoil

Flow around the RAE2822-airfoil (Cook *et al.* 1979) has been computed for the Case 9 flow condition: $M = 0.734$, $Re = 6.5 \times 10^6$, and $\alpha = 2.54^o$. In this case a shock interacts with the viscous boundary layer. It is, however, not strong enough to induce separation. The flow transitions at 3% on the upper and lower surfaces. The computational mesh consists of 256x64 cells. It has been taken from EUROVAL (Haase *et al.* 1993).

2.3.4 Results for flow computation around airfoils

Pressure and skin friction distributions on wing and flap are shown in Fig. 1 for flow over the NLR7301-airfoil at $\alpha = 13.1^o$ incidence. The wing and flap profiles are shown in the background of the plots. The pressure distribution agrees well with the experiments for the S-A, SST, and v^2-f Model 1. Model 2, however, significantly over-predicts the pressure on the suction surface of the flap. The pressure discrepancy in the suction peak of the wing is even larger but not as visible on the plot because of the difference in the C_p scale resolution.

Model 2 also overpredicts the skin friction over the largest part of the wing. It predicts, however, a larger skin friction rise downstream of transition. In this computation transition is fixed for all models by switching off production terms in the turbulent transport equations at $x/c = 0.035$ on the upper wing surface, at 0.709

on the lower wing surface, and at 1.076 on the upper flap surface. The handling of the v^2-f source terms is described in a previous paper (Kalitzin 1997, 1998). Note, the results do depend on the location where transition is being fixed. Moving the transition location even in the limits, it has been observed in the experiments, changes the strength of the laminar separation bubble upstream of transition, affecting mainly velocity and skin friction predictions. Numerical dissipation, which is desired in the transition region to smooth out instabilities caused by the ad hoc transition fixing, is a dominant factor in this region.

However, similar differences in the results can also be observed for a fully turbulent flow computation shown in Fig 2. While the pressure distribution remains largely unaffected, the computation does not predict the laminar separation bubble. As before, the skin friction is overpredicted on the upper surface of the wing by Model 2. The boundary layer is for all models thicker for a fully turbulent computation than a computation with transition, as shown with velocity profiles at Station 14 in Fig. 3c and Fig. 3b. Station 14 is located on the upper surface of the flap near the trailing edge at $x/c = 1.2$. In both cases, Model 2 predicts a boundary layer that is too thick on the suction side of the airfoil. Note that natural transition on the pressure surface of the wing occurs significantly further upstream than the location observed in the experiments and varies with the turbulence model used.

At lower angle of attack, the difference between the models becomes smaller as shown in Fig. 4 for flow at $\alpha = 6.0^o$ incidence. While the skin friction remains about the same as for the $\alpha = 13.1^o$ case, the pressure increases drastically in the suction peak region of the wing. Note, the skin friction does not become negative in the transition region on the upper surface of the wing as the computations carried out do not predict a laminar separation bubble. As for the $\alpha = 13.1^o$ case, the skin friction is overpredicted with Model 2 on the upper surface of the wing.

Model 1 predicts considerable better results and is in closer agreement with the S-A and SST models. The major difference between Model 1 and Model 2 is the definition of the coefficient $C_{\epsilon 1}$ and the value for C_μ. The profile of the coefficient $C_{\epsilon 1}$ over the boundary layer is shown in Fig. 3a for Station 8 for the flow over the NLR7301-airfoil at $\alpha = 13.1^o$. Station 8 is located on the upper surface of the wing near the trailing edge at $x/c = 0.94$. For this station the boundary layer is about $y/c = 0.04$ thick. The coefficient $C_{\epsilon 1}$ in Model 1 changes smoothly from 1.55 at the wall to 1.3 in the free-stream. Eq. (3) is defined in such a way that the value for $C_{\epsilon 1}$ is bounded between these to values. For Model 2, in contrast, $C_{\epsilon 1}$ has a value of 1.44 in the larger part of the boundary layer with a value of 1.64 at the wall. The higher value of $C_{\epsilon 1}$ away from the wall leads to a larger production of ϵ on the outer edge of the boundary layer, decreasing the eddy viscosity there. This causes the boundary layer to grow more rapidly for flows with strong adverse pressure gradients. The larger skin friction on the upper surface predicted with Model 2 might be related to an overprediction of turbulent kinetic energy in the logarithmic layer which is proportional to the wall skin friction. A comparison of $C_{\epsilon 1}$ at Station 8 shows lower values for Model 2 in the first quarter of the boundary layer outside of the laminar sublayer.

All models considered fail to predict or do not predict enough separation for the A-airfoil as shown in Fig. 5. Corresponding to the velocity profile at $x/c = 0.96$, the v^2-f Model 2 predicts again a larger boundary layer thickness on the suction side of the airfoil. The station for $x/c = 0.96$ is located on the upper surface of the airfoil near the trailing edge. In this case the pressure in the suction peak and the velocity profiles are closer to experimental data for Model 2 rather than for the original Model 1. In Haase *et al.* (1997) it is shown that more separation close to the trailing edge increases the pressure in the suction peak. Consistently, the pressure in the suction peak is slightly higher for Model 2.

Significantly more separation has been obtained with the v^2-f model for this test case during the 1996 CTR-Summer Program by Lien (1996). However, in that computation the coefficient for $C_{\epsilon 1}$ has been set to 1.55. As discussed before this leads to thicker boundary layers in flows with adverse pressure gradients. In the general case, however, a lower value of $C_{\epsilon 1}$ is required in the free stream.

Consistent with the NLR7301 cases, the skin friction is overpredicted on the suction side of the airfoil with Model 2. Model 1 predictions are similar to those obtained with the S-A model. The SST model is here closest to the experimental data. It has been found that for the A-airfoil results are less dependent on the location where transition is fixed than for the NLR7301, 13.1^o case.

The same Fig. 5 contains pressure, skin friction distributions, and velocity profiles at one station for flow over the RAE2822-airfoil for Case 9. The plots contain results obtained with the S-A and v^2-f Model 1, 2, and 3. Comparison of S-A, SST, and v^2-f Model 2 results for Case 9 and Case 10 are published in Kalitzin (1999).

While there is hardly any difference in the pressure distribution and shock location for all three different v^2-f versions, the skin friction is significantly overpredicted by Model 3 downstream of the shock. Both Model 2 and Model 3 predict larger skin friction on the lower surface of the airfoil while Model 1 agrees well with the S-A result. It is interesting to note the difference of the velocity profile close to the wall computed with Model 3. Station $x/c = 0.9$ is on the upper surface of the airfoil between the shock and the trailing edge. The larger skin friction for Model 3 corresponds here to a larger velocity gradient at the wall.

2.4 Subsonic three-element trapezoidal wing-body

Computation of flow around a three-element trapezoidal wing-body has been chosen to test the performance of the v^2-f model in three-dimensional flow around complex geometries. A multigridable, multiblock mesh consisting of 25 blocks with about 8 million grid points has been provided by the Subsonic Aerodynamics Branch at NASA Langley (Jones *et al.* 1998). The communication between the blocks includes one-to-one cell communication and patched interpolation.

Initial tests estimated that CFL3D, version 5, requires about 450 Mw of memory for a v^2-f computation with a two-factored Approximate Factorization scheme on a Cray C90. This amount of memory is cheaply available only on a parallel machine. A parallel version of CFL3D, version 6, which is now in development at Langley, allows the run of one or more blocks on one processor. The bulk of cells in the mesh provided is unevenly concentrated in 4 blocks as shown in Fig. 6b. This makes the

computation with this mesh with CFL3D highly inefficient on a parallel machine. A new topology with 72 blocks has been obtained by splitting the largest blocks. The surface mesh of this new grid is shown in Fig. 6a. The different grey shades indicate the faces belonging to different blocks.

Preliminary computations have been carried out on a mesh obtained from the second multigrid level consisting of 898640 cells for the flow conditions: $M = 0.2$, $Re = 4.3 \times 10^6$, and $\alpha = 10.0^o$. Computations with the v^2-f and S-A models have been carried out on ALPHA PC's using about 420 MB of memory. A two-factored AF scheme is used for the v^2-f computation in the blocks containing the wing-body junction while a three-factored scheme is used elsewhere.

Pressure distributions on cuts at 28% and 95% span are shown for fully turbulent computation in Fig. 7. Both plots show that the pressure on the suction side is not adequately predicted. Discrepancies at this angle of attack are a consequence of grid coarseness. The discrepancy between experimental data and computation is larger towards the tip. A wing tip vortex generates additional lift by lowering the pressure above the tip. The presence of the vortex requires an even larger grid resolution. Nash & Roger (1999) have made a grid dependency study for the same configuration. They estimated that at least 6 million grid nodes are required to obtain a mesh independent value for the lift coefficient at a 30-degree angle of attack.

Note that to obtain the pressure cuts the slat and flap have been rotated to zero degree deflection. The wing has been cut with planes parallel to the symmetry plane. The obtained data and the corresponding experimental data have then been transformed by rotating the slat and flap back into their original position.

3. Summary and future plans

Results obtained for flow around airfoils show significant differences for the different versions of the v^2-f model. The original version, which uses the wall distance albeit for varying the coefficient $C_{\epsilon 1}$, predicts the best results in general. In particular, for high Reynolds number flows and flow regions which are close to separation, the original version predicts consistently better skin friction distributions.

A closer look will be taken to understand whether these differences are just a matter of model tuning or whether the coefficient $C_{\epsilon 1}$ has to depend on the wall distance. Collaborative work with Petros Koumoutsakos (ETH Zürich) is underway to optimize the coefficients of the v^2-f model using an evolution algorithm. In the initial phase, several test cases ranging from flow over a flat plate to high Reynolds number flow with adverse pressure gradients are set up to reproduce the existing coefficients of Model 1. Modifications to the model will be considered in later stages of the work.

The work on the three-element wing-body is well in progress. The test case is set up for the new parallel version 6 of CFL3D. Work is underway to implement the v^2-f model into this version. A major part of work for this test case has consisted so far in writing post- and pre-processing tools which split the major blocks in smaller blocks and tools which automatically determine the topology of the new grid generating a communication input file for CFL3D.

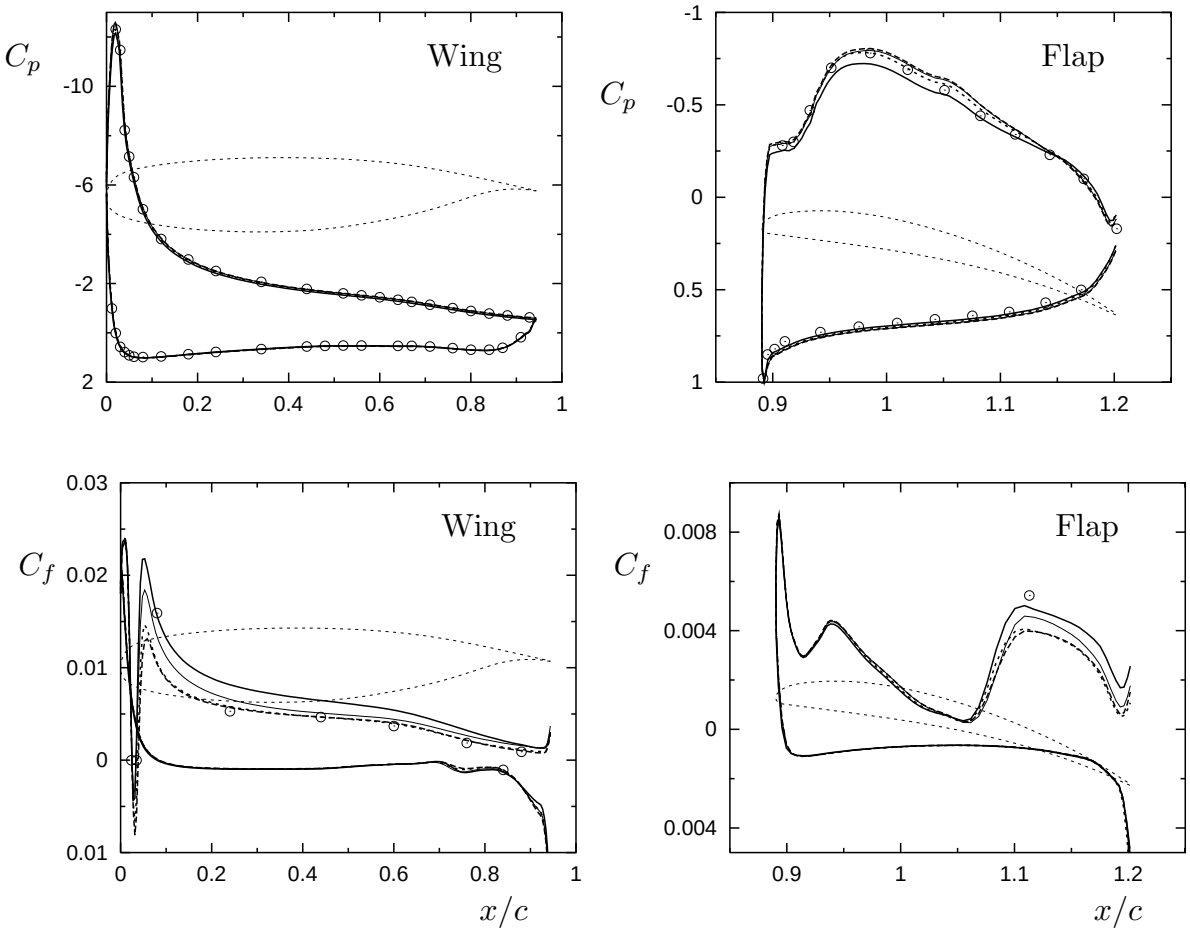

FIGURE 1. NLR7301-airfoil, $\alpha = 13.1^o$; pressure and skin friction distribution; ——— : v^2-f Model 2, – – – – : S-A, ····· : SST, ——— : v^2-f Model 1, ∘ : Exp.

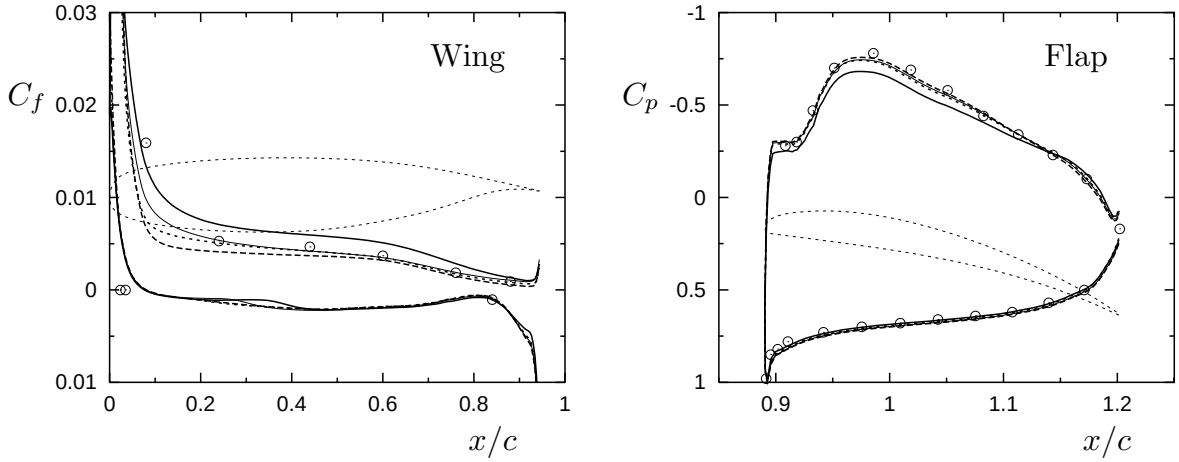

FIGURE 2. NLR7301-airfoil, $\alpha = 13.1^o$; pressure and skin friction distribution for fully turbulent computation; ——— : v^2-f Model 2, – – – – : S-A, ····· : SST, ——— : v^2-f Model 1, ∘ : Exp.

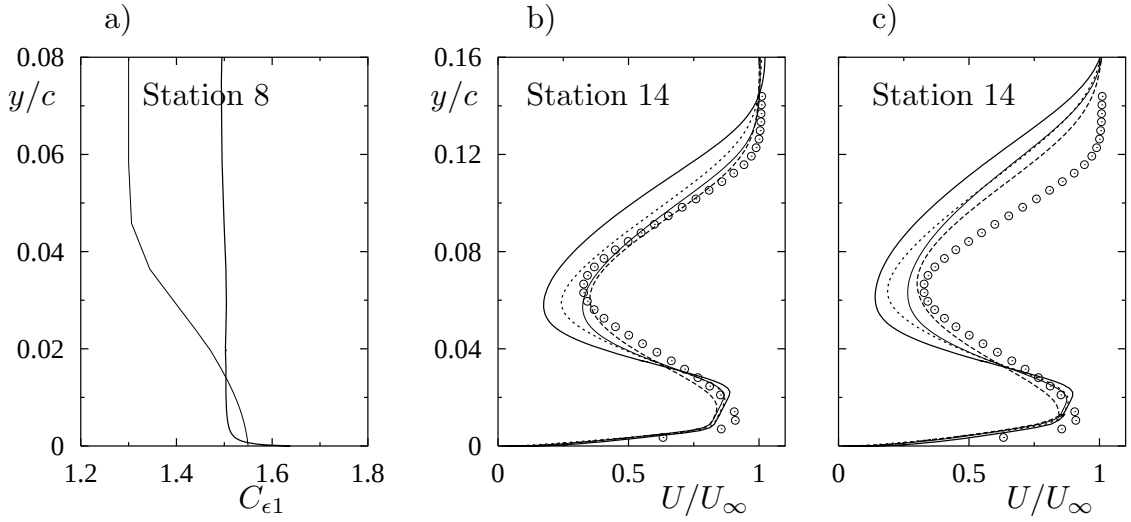

FIGURE 3. NLR7301-airfoil, $\alpha = 13.1^o$; $C_{\epsilon 1}$ and velocity profiles: a) and b) computation with transition fixed; c) fully turbulent computation; ——— : v^2-f Model 2, - - - - : S-A, ····· : SST, ——— : v^2-f Model 1, ○ : Exp.

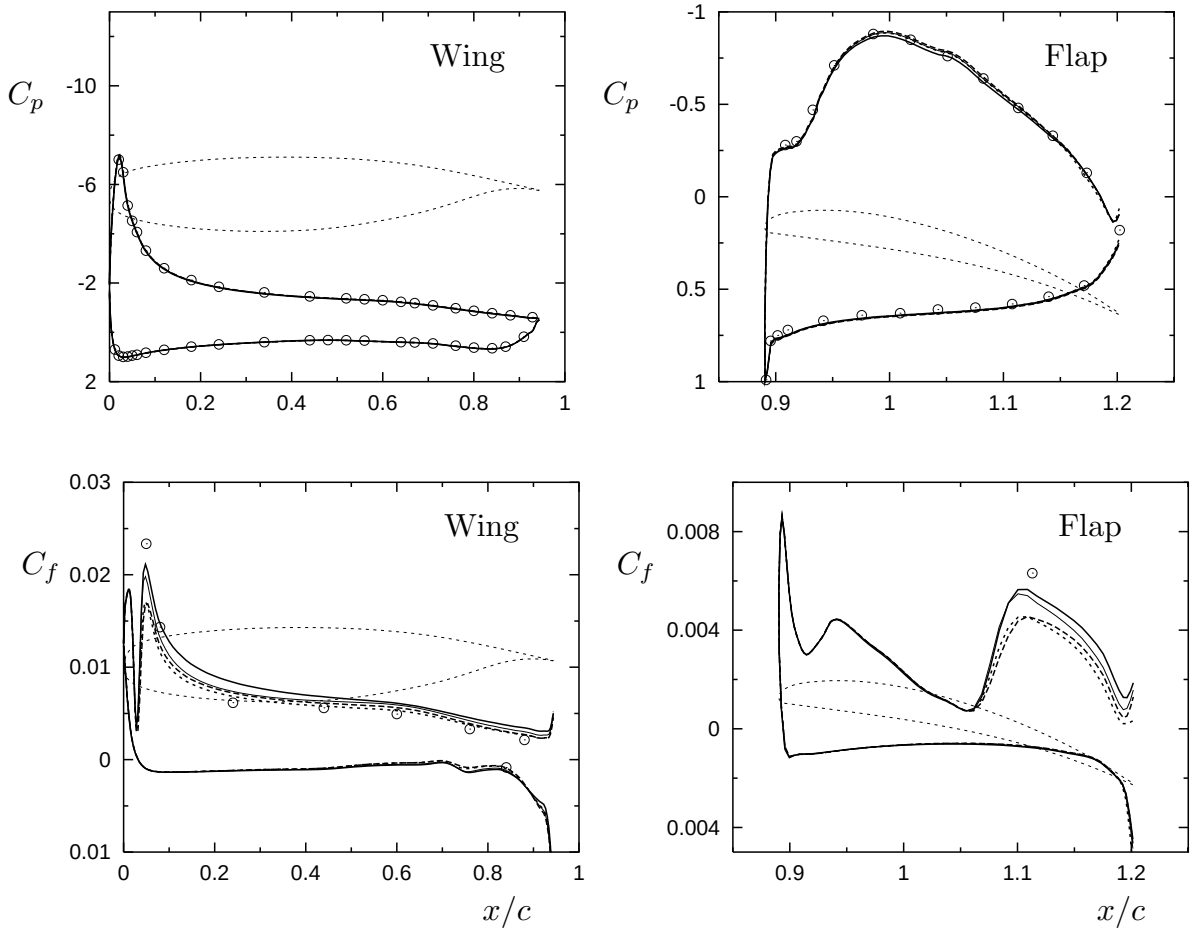

FIGURE 4. NLR7301-airfoil, $\alpha = 6.0^o$; pressure and skin friction distribution; ——— : v^2-f Model 2, - - - - : S-A, ····· : SST, ——— : v^2-f Model 1, ○ : Exp.

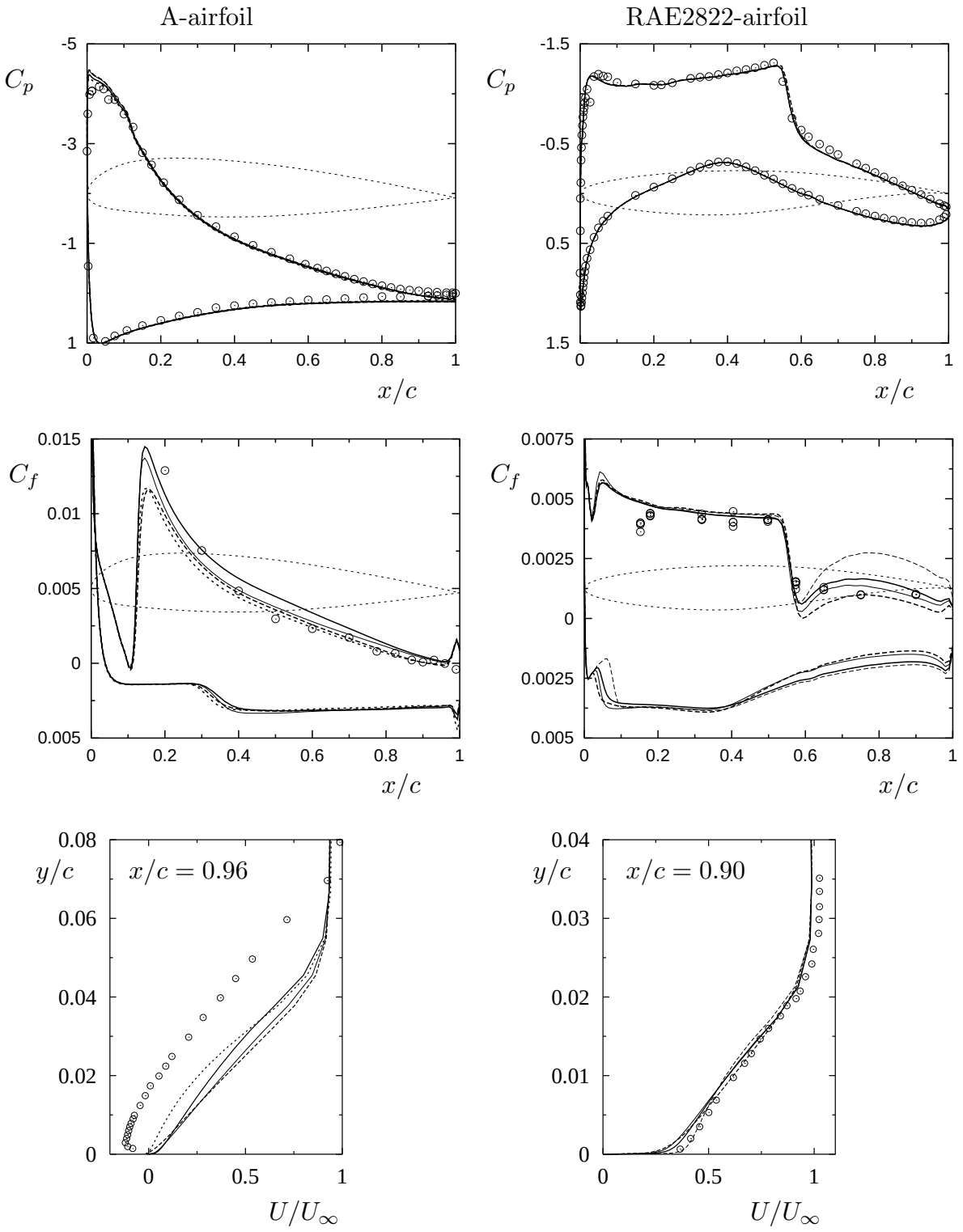

FIGURE 5. A- and RAE2822-airfoils; pressure, skin friction distribution and velocity profiles; ——— : v^2-f Model 2, - - - - : S-A, ····· : SST, ——— : v^2-f Model 1, – – – – : v^2-f Model 3, ○ : Exp.

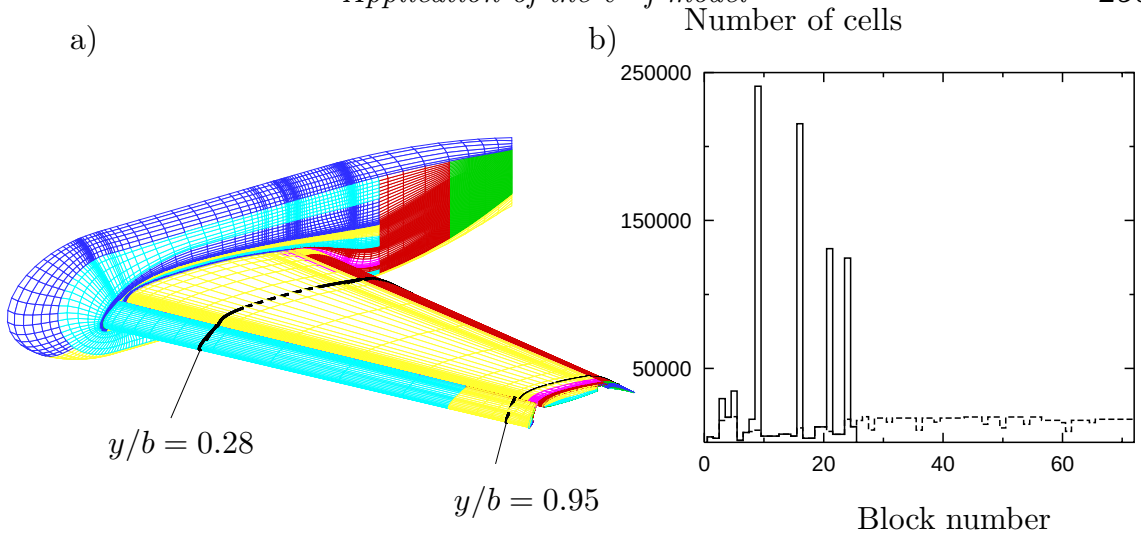

FIGURE 6. Trapezoidal wing-body; multiblock surface mesh and number of cells in each block for ——— : 25 and - - - - : 72 block mesh

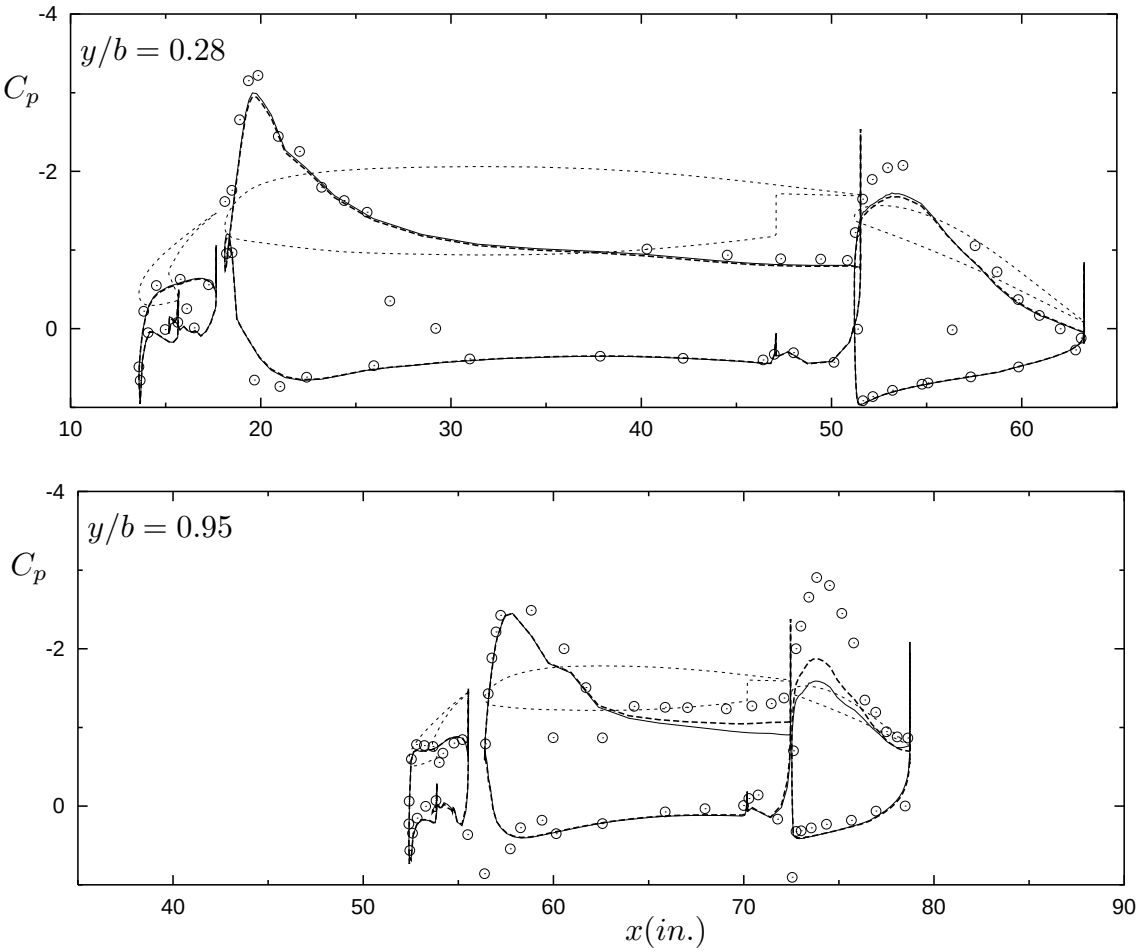

FIGURE 7. Trapezoidal wing-body; pressure distribution on slat, wing and flap; - - - - : S-A, ——— : v^2-f Model 1, ○ : Exp.

Acknowledgments

The author would like to acknowledge W. B. Compton for providing the three-element wing-body mesh and W. Haase for providing the airfoil meshes.

REFERENCES

Van den Berg, B. 1979 Boundary layer measurements on a two-dimensional wing with flap. *NLR TR 79009 U.*

Cook, P. H., McDonald, M. A. & Firmin, M. C. P. 1979 Aerofoil 2822 - Pressure Distributions, Boundary Layer and Wake Measurements. *AGARD AR 138.*

Durbin, P. 1995 Separated flow computations with the $k-\epsilon-\overline{v^2}$ model. *AIAA J.* **33,** 659-664.

Glayzes, Ch. 1989 Opération décrochage - Résultats de la 2ème campangne d'essais à F2 - Mesures de pression et vélocimétrie laser. *RT-DERAT 55/5004.*

Haase, W., Bradsma, F., Elsholz, E., Leschziner, M., & Schwamborn D. 1993 EUROVAL-an European Initiative on Validation of CFD Codes. *Notes on Numerical Fluid Mechanics, Vol.* **42***, Vieweg.*

Haase, W. , Chaput, E., Elsholz, E., Leschziner, M. & Müller, U. R. 1997 *ECARP - European Computational Aerodynamics Research Project: Validation of CFD Codes and Assessment of Turbulence Models.* Vol. **58**, Vieweg.

Jones, K. & Compton, W. B. 1998 Private communications.

Kalitzin, G. 1999 Application of v^2-f turbulence model to transonic flows. *AIAA-99-3780.*

Krist, S., Biedron, R. & Rumsey, C. 1998 CFL3D User's Manual (Version 5.0). *NASA/TM-1998-208444.*

Lien F. S. & Durbin P. A. 1996 Non-linear $k-\epsilon-v^2$ modeling with application to high-lift. *Summer Program Proceedings.* Center for Turbulence Research, NASA/Stanford Univ., 5-22.

Lien F. S., Kalitzin, G. & Durbin, P. A. 1998 RANS modeling for compressible and transitional flows. *Summer Program Proceedings.* Center for Turbulence Research, NASA/Stanford Univ., 267-286.

Menter, F. R. 1993 Zonal two equation $k-\omega$ turbulence model predictions. *AIAA Paper No. 93-2906.*

Nash, S. M. & Roger, S. E. 1999 Numerical study of a trapezoidal wing high-lift configuration. *AIAA Paper No. 1999-01-5559.*

Parneix, S. & Durbin, P. 1997 Numerical simulation of 3D turbulent boundary layers using the V2F model. *Annual Research Briefs.* Center for Turbulence Research, NASA/Stanford Univ. 135-148.

Spalart, P. R. & Allmaras, S. R. 1992 A one-equation turbulence model for aerodynamic flows. *AIAA 92-439.*